Inverse transfer of magnetic helicity in supersonic magnetohydrodynamic turbulence

J.-M. Teissier and W.-C. Müller

Technische Universität Berlin, ER 3-2, Hardenbergstr. 36a, D-10623 Berlin, Germany

E-mail: `jm.teissier@astro.physik.tu-berlin.de`

Abstract. The inverse transfer of magnetic helicity is studied through a fourth-order finite volume numerical scheme in the framework of compressible ideal magnetohydrodynamics (MHD), with an isothermal equation of state. Using either a purely solenoidal or purely compressive mechanical driving, a hydrodynamic turbulent steady-state is reached, to which small-scale magnetic helical fluctuations are injected. The steady-state root mean squared Mach numbers considered range from 0.1 to about 11. In all cases, a growth of magnetic structures is observed. While the measured magnetic helicity spectral scaling exponents are similar to the one measured in the incompressible case for the solenoidally-driven runs, significant deviations are observed even at relatively low Mach numbers when using a compressive driving. A tendency towards equipartition between the magnetic and kinetic fields in terms of energy and helicity is noted. The joint use of the helical decomposition in the framework of shell-to-shell transfer analysis reveals the presence of three distinct features in the global picture of a magnetic helicity inverse transfer. Those are individually associated with specific scale ranges of the advecting velocity field and commensurate helical contributions.

1. Introduction

Magnetic helicity $\mathcal{H}^M = \int \mathbf{a} \cdot \mathbf{b} dV$ (with the magnetic vector potential $\mathbf{a}, \mathbf{b} = \nabla \times \mathbf{a}$) is an ideal invariant of the magnetohydrodynamics (MHD) equations [11, 27]. It quantifies topological aspects of the magnetic field lines, such as their interlinkage, twist, writhe and knotedness and is approximately conserved even during reconnection events [23, 4]. This implies significant constraints on the dynamics of many astrophysical systems. For example, both hemispheres of the sun present helical magnetic fields, with opposite signs [4]. These helical fields are known to play an important role for the dynamics of solar flares and coronal mass ejections [19]. Magnetic helicity is also transferred to the interplanetary medium through the solar wind [5]. Another key property of magnetic helicity is that it exhibits an inverse transfer in Fourier space [25], i.e. it is transferred from small to larger scales, which makes its study relevant for the theory of magnetic dynamo processes and the formation of large-scale magnetic structures in general [7].

Because of the nearly vanishing molecular dissipation in space, astrophysical systems are generally expected to be in a turbulent state, often accompagnied by supersonic fluid motion with Mach numbers of up to 10 and beyond, see e.g. [17, 10]. Therefore the present investigation applies a recently developed higher-order constrained-transport scheme to evolve the MHD Euler equations in a triply periodic configuration to study the spectral dynamics of magnetic helicity under supersonic flow conditions [26].

The inverse transfer of magnetic helicity has been studied in the deeply subsonic, incompressible case in references [21, 24], where it has been observed that the magnetic helicity spectrum exhibits a power-law behaviour, with $H_k^M \sim k^{-3.3}$ in the inverse transfer range. A dynamic balance involving the magnetic and kinetic energy and their helicities has been observed, as well. A study of shell-to-shell magnetic helicity transfer rates [1] has shown, in addition, that local and non-local transfer processes coexist in incompressible MHD turbulence. The inverse transfer has also been recently studied using the so-called "helical decomposition", a decomposition in eigenfunctions of the curl operator in Fourier space [18].

However, regarding the inverse transfer in compressible turbulence, only the subsonic and the mildly supersonic case have been investigated so far [2, 6, 8]. The present work considers high Mach number turbulence in the ideal isothermal MHD framework. The inverse transfer of magnetic helicity is studied by injecting magnetic helical fluctuations at small scales in a steady state of large-scale driven hydrodynamic turbulence, as described in section 2. Section 3 introduces the applied analysis tools, namely the helical decomposition and the shell-to-shell transfers, which are used to shed some light on the magnetic helicity inverse transfer and the role of compressibility. The simulation results are discussed in section 5, after having considered in section 4 general aspects of the inverse transfer, including the growth of magnetic structures and the observation of scaling exponents in Fourier space. Section 6 concludes with a summary.

2. Numerical experiments

The ideal compressible MHD equations, using an isothermal equation of state, read:

$$\partial_t \rho = -\nabla \cdot (\rho \mathbf{v}), \tag{1}$$

$$\partial_t(\rho \mathbf{v}) = -\nabla \cdot \left(\rho \mathbf{v}\mathbf{v}^T + (p + \frac{1}{2}|\mathbf{b}|^2)I - \mathbf{b}\mathbf{b}^T \right), \tag{2}$$

$$\partial_t \mathbf{b} = \nabla \times (\mathbf{v} \times \mathbf{b}), \tag{3}$$

$$\nabla \cdot \mathbf{b} = 0, \tag{4}$$

with ρ the mass density, $\mathbf{v}$ the velocity, $p = \rho c_s^2$ the isothermal pressure with c_s the constant sound speed, $\mathbf{b}$ the magnetic field and I the 3×3 identity matrix. These equations are solved through a fourth-order finite-volume scheme described in reference [26]. The magnetic field solenoidality is preserved up to machine precision through a constrained-transport approach [12]. As strong shocks are common in supersonic runs and lead to stability issues for higher-order numerical methods, the robustness of the scheme is enhanced by resorting to lower-order reconstruction methods in their vicinity. This procedure is called "flattening" or "fallback approach" [9, 3, 26].

The runs are performed in a triply periodic cubic box of size $L = 1$, at resolution 512^3, with an isothermal sound speed of $c_s = 0.1$.

Starting with a fluid at rest, a large scale mechanical forcing drives the plasma until a statistical steady-state with a desired root mean squared (RMS) Mach number $\mathcal{M}$ is reached. This driving is done through an Ornstein-Uhlenbeck process either with a purely solenoidal or purely compressive driving (in a way similar to references [14, 13]). The wavenumbers for which $1 \leq |\mathbf{k}|/\kappa < 3$, with $\kappa = \frac{2\pi}{L}$ the smallest wavenumber in the system, are forced and the acceleration field in configuration space is normalised so that a constant kinetic energy injection rate ϵ_{inj}^K is achieved. This normalisation is done in order to control exactly the magnetic-to-kinetic injection ratio, see below. The forcing autocorrelation time is constant, set to the turbulent turnover time $t_{\mathcal{T}} = \frac{L}{2c_s\mathcal{M}^*}$ with $\mathcal{M}^*$ an *a priori* estimate of the expected RMS Mach number (based on the empirical relation between ϵ_{inj}^K and $\mathcal{M}$ given in reference [20]). This forcing

generates a weak mean velocity field which is removed at each iteration, since the magnetic field is not Galilean invariant.

Five solenoidally and four compressively driven runs are considered. The (s)olenoidally-driven runs, labelled with an "s", have steady-state Mach numbers of $\mathcal{M} \approx 0.116, 1.09, 5.06, 7.03$ and 11.1 for the M01s, M1s, M5s, M7s and M11s runs respectively. The (c)ompressively-driven runs M1c, M3c, M5c and M8c exhibit steady-state Mach numbers of $\mathcal{M} \approx 0.797, 2.80, 5.05$ and 7.87 respectively.

When the steady-state is reached, magnetic helical fluctuations with maximum helical fraction are injected at the wavenumbers $48 \leq K < 53$, with $K = |\mathbf{k}|/\kappa$. The magnetic energy injection rate ϵ_{inj}^M is constant and such that $R_{inj} = \epsilon_{inj}^M/\epsilon_{inj}^K$ is equal to unity for all the runs but the M01s and M1s ones, for which $R_{inj} = 4$ and $R_{inj} = 2$ respectively. This increased R_{inj} has been chosen in order to observe faster convergence of the inverse transfer scaling laws.

3. Analysis tools

The magnetic helicity transfers are analysed using jointly a shell-to-shell transfer formalism [1, 16] and the so-called "helical decomposition"[18], where the fields are projected in Fourier space along a basis formed by the eigenvectors of the curl operator [7]:

$$\hat{\mathbf{h}}_{\mathbf{k}}^{\pm} = \frac{1}{\sqrt{2}} \frac{\mathbf{k} \times (\mathbf{k} \times \hat{\mathbf{e}}) \mp ik(\mathbf{k} \times \hat{\mathbf{e}})}{k^2 \sqrt{1 - (\mathbf{k} \cdot \hat{\mathbf{e}}/k)^2}}, \tag{5}$$

where $\hat{\mathbf{e}}$ is an arbitrary unitary vector non-parallel to $\mathbf{k}$. These eigenvectors verify $i\mathbf{k} \times \hat{\mathbf{h}}_{\mathbf{k}}^{\pm} = \pm k\hat{\mathbf{h}}_{\mathbf{k}}^{\pm}$. A third eigenvector of the curl operator is $\mathbf{k}/k$, which corresponds to compressive modes and is associated with the eigenvalue 0. The three vectors $(\mathbf{k}/k, \hat{\mathbf{h}}_{\mathbf{k}}^{+}, \hat{\mathbf{h}}_{\mathbf{k}}^{-})$ form an orthonormal basis in Fourier space, on which the magnetic and velocity field can be projected, before being transformed in configuration space. The resulting fields are denoted $\mathbf{b}^P$, $\mathbf{v}^P$ for the (p)ositive helical parts of the magnetic and velocity fields, which results from a projection along $\hat{\mathbf{h}}_{\mathbf{k}}^{+}$. Similarly, $\mathbf{b}^N$ and $\mathbf{v}^N$ are their (n)egative helical parts (projection along $\hat{\mathbf{h}}_{\mathbf{k}}^{-}$). The compressive part of the velocity field is denoted $\mathbf{v}^C$.

The shell-to-shell magnetic helicity transfer function defined in reference [1] is thus extended to:

$$\mathcal{T}_{s_K s_P s_Q}^{\mathcal{H}^M}(Q, P, K) = 2 \int \mathbf{b}_K^{s_K} \cdot (\mathbf{v}_P^{s_P} \times \mathbf{b}_Q^{s_Q}) dV, \tag{6}$$

where the subscripts $s_K, s_Q \in \{P, N\}$ correspond to the positive and negative helical parts of the magnetic field and $s_P \in \{P, N, C\}$ for the velocity field, so that twelve combinations are possible. The K, P, Q subscripts stand for the shell-decomposed fields. For example, $\mathbf{b}_K^{s_K}$ corresponds to the s_K-helical part of the magnetic field in configuration space, but keeping only the modes so that $K \leq |\mathbf{k}|/\kappa < K + 1$ with $\kappa = \frac{2\pi}{L}$ the smallest wavenumber in the system. For $s_K = s_Q$, the antisymmetric property $\mathcal{T}_{s_K s_P s_K}^{\mathcal{H}^M}(Q, P, K) = -\mathcal{T}_{s_K s_P s_K}^{\mathcal{H}^M}(K, P, Q)$ allows to interpret these terms as the transfer rate of magnetic helicity from shell Q to shell K of the $\mathbf{b}^{s_Q}$ field, mediated by the $\mathbf{v}^{s_P}$ field at shell P. When $s_K \neq s_Q$, the terms have to be considered pairwise to verify this antisymmetric property.

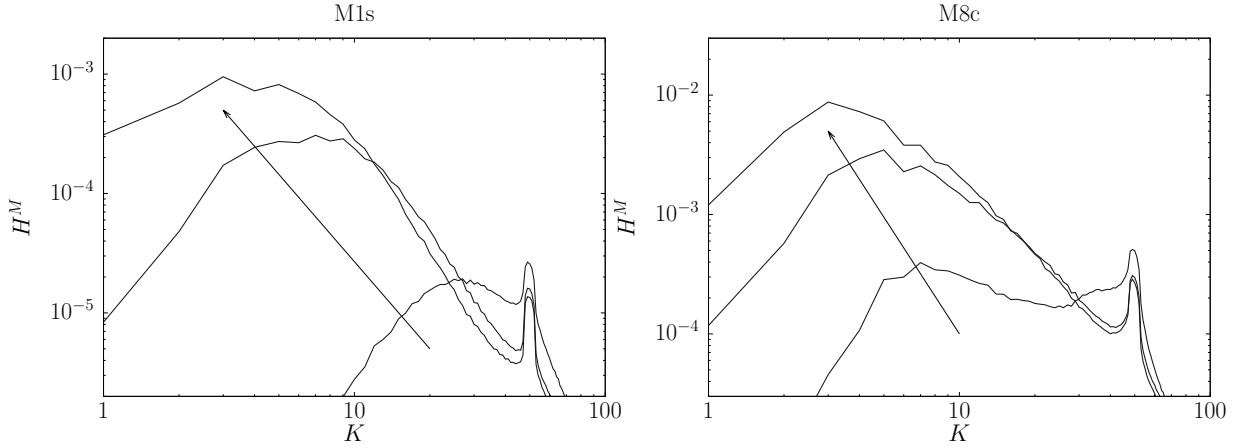## 4. Growth of magnetic structures and scaling laws

Figure 1. Time evolution of the magnetic helicity spectra for the M1s and M8c runs.

As in the incompressible case, the growth of magnetic structures is observed in the highly supersonic isothermal case. This is shown through the development to smaller wavenumbers of the magnetic helicity spectra H^M in figure 1 for the M1s and M8c runs. Figure 2 shows the time evolution of magnetic helicity slices using the Coulomb gauge ($\nabla \cdot \mathbf{a} = 0$) for the M8c run.
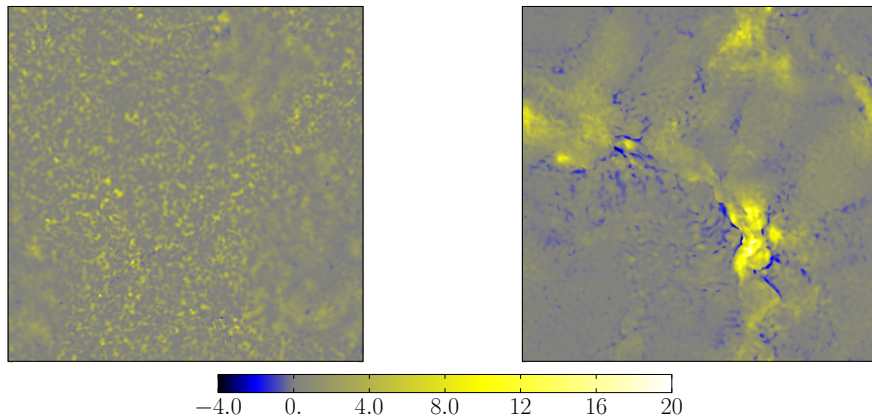

Figure 2. Magnetic helicity density slices at an early (left) and later (right) instant in time, for the M8c run. The values are normalised by the mean magnetic helicity density in the system.

The magnetic helicity Fourier spectra exhibit scaling laws with an exponent relatively close to -3.3 for all the solenoidally-driven runs, even for a RMS Mach number as high as 11 (figure 3.(a)). A least-squares fit in the region $20 \leq K \leq 30$ gives indeed $H^M \sim K^m$ with $m \approx -3.3, -3.3, -3.2, -3.1, -3.0$ for the M01s, M1s, M5s, M7s and M11s runs respectively, when considering spectra at the instant in time when the magnetic helicity integral scale $\mathcal{I}_{\mathcal{H}^M} = \int_K K^{-1} H^M dK / \int_K H^M dK$ is close to $\frac{L}{6}$. These values are close to the -3.3 one observed in the incompressible case [24]. However, for the compressively-driven runs (figure 3.(b)), even though the scaling exponent is close to -3.3 for the M1c run, clear departures are already visible for the M3c run for which $\mathcal{M} \approx 2.80$. The spectral index measured through a least squares fit

in the region $15 \leq K \leq 25$ gives $H^M \sim K^m$ with $m \approx -3.2, -2.6, -2.2, -2.3$ for the M1c, M3c, M5c and M8c runs respectively, for the spectra at the instant when $\mathcal{I}_{\mathcal{H}^M} = \frac{L}{6}$.
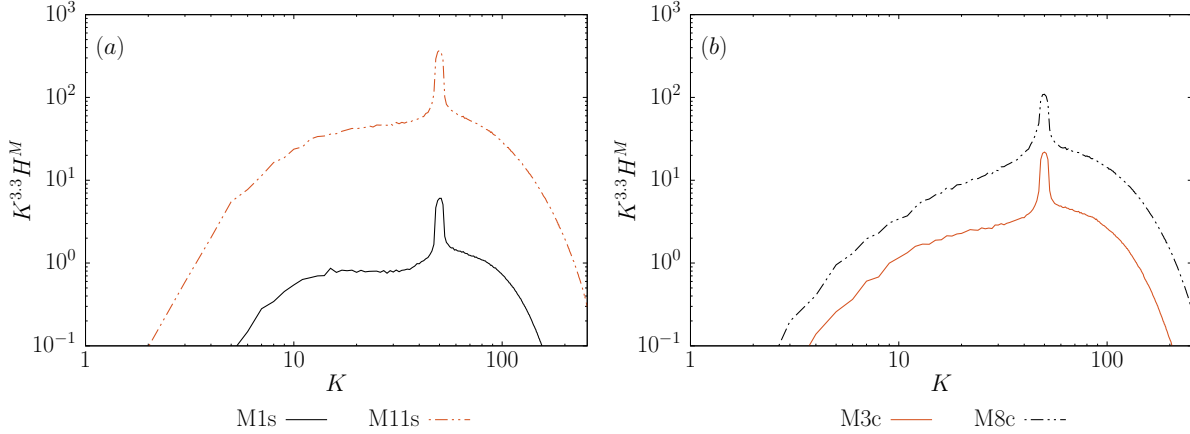

Figure 3. Magnetic helicity spectra for the M1s, M11s, M3c and M8c runs at the instant when $\mathcal{I}_{\mathcal{H}^M} = \frac{L}{6}$, compensated by $K^{3.3}$.

In several numerical experiments involving helical fields, a tendency towards equipartition both in terms of magnetic and kinetic energies as well as in terms of current and kinetic helicities has been reported. Namely, the specific kinetic energy spectrum E^V (which is the same as the kinetic energy spectrum in the incompressible case), the magnetic energy spectrum E^M, the kinetic helicity spectrum H^K and the current helicity spectrum $H^J = K^2 H^M$ have been found to verify the following balance [22, 15, 24]:

$$\left(\frac{E^V}{E^M}\right)^\gamma \propto \frac{H^K}{H^J}, \tag{7}$$

in a certain spectral range. While references [22, 15] observed this balance for $\gamma = 1$ in the direct transfer region, reference [24] found that an exponent $\gamma = 2$ would be more consistent with the experimental data in the inverse transfer region. For the compressible runs presented here, a good agreement with the experimental data has been found for:

$$\left(\frac{E^{V,sol}}{E^{A,sol}}\right)^\gamma \propto \frac{H^K}{H^A}, \tag{8}$$

with $E^{V,sol}$ the solenoidal part of the velocity power spectrum, $E^{A,sol}$ the solenoidal part of the Alfvén velocity power spectrum and H^A the "Alfvénic helicity spectrum", that is, the spectrum of $\mathcal{H}^A = \int \mathbf{v_A} \cdot (\nabla \times \mathbf{v_A}) dV$. The rationale behind this extension of relation (7) comes from the fact that the incompressible exponent of -1.3 [24] for the current helicity H^J is retrieved even at high compressibility when considering H^A (see figure 4). The energies associated with the Alfvénic and kinetic helicities are then the *solenoidal parts* of the corresponding velocity power spectra. For this choice, plotting $\left(\frac{E^{V,sol}}{E^{A,sol}}\right)^\gamma \frac{H^A}{H^K}$ as a function of K gives a small spread between the curves for both the least compressible (the M01s, M1s and M1c) and the most compressible (the M3c, M5c and M8c) runs. Other relations have been tested, considering for example the magnetic energy spectrum, the power spectrum of $\mathbf{w} = \sqrt{\rho} \mathbf{v}$, or the co-spectrum of velocity and momentum. Several of these empirical relations are approximately verified in the inverse transfer region, but the best agreement with the experimental data has been obtained with relation (8) so far. These other choices seem furthermore to lead to a higher spread of the

curves. For the low Mach number M01s, M1s and M1c runs, relation (8) is well followed with $\gamma = 2$ in the spectral region $15 \leq K \leq 40$, with a constant close to 1.1 ± 0.3. For the highly compressible M3c, M5c and M8c runs, relation (8) is well followed with $\gamma = 1$ in the region $16 \leq K \leq 31$, with a constant close to 2.7 ± 0.5. The M5s, M7s and M11s runs present an intermediate behaviour.
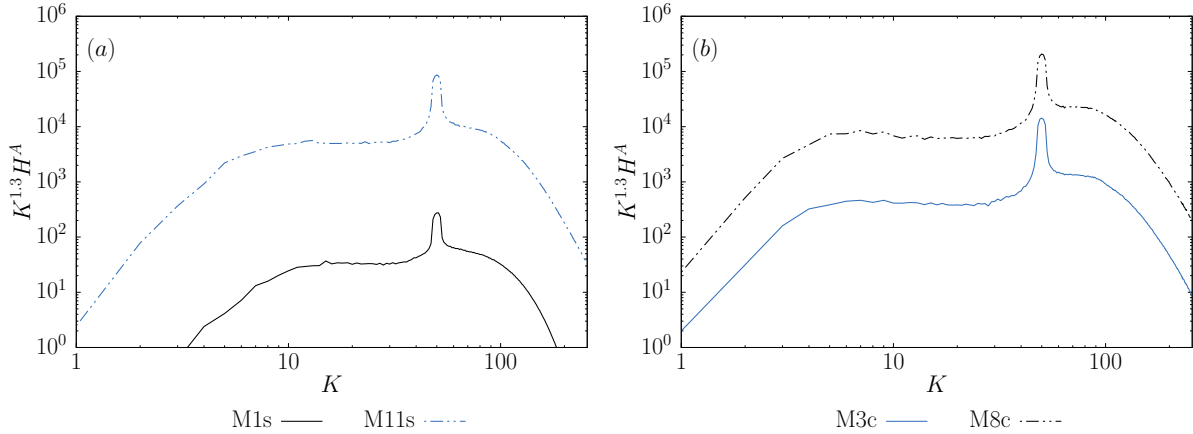

Figure 4. "Alfvénic helicity" spectra for the M1s, M11s, M3c and M8c runs at the instant when $\mathcal{I}_{\mathcal{H}^M} = \frac{L}{6}$, compensated by $K^{1.3}$.
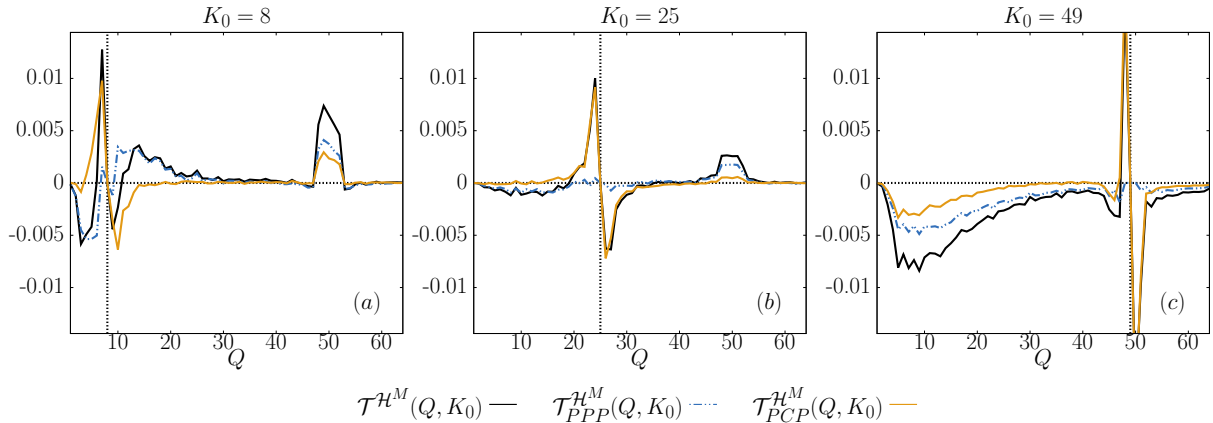
5. Shell-to-shell helical transfers

Figure 5. Magnetic helicity transfer rates from shell Q to shell $K_0 \in \{8, 25, 49\}$ at the instant when $\mathcal{I}_{\mathcal{H}^M} = \frac{L}{10}$. The black curve is the total transfer rate, sum of the twelve helical contributions, whereas the other ones correspond to the dominant PPP and PCP helical contributions. A positive (negative) value means that shell Q gives (receives) magnetic helicity to (from) shell K_0. The transfer rates are normalised by the magnetic helicity injection rate.

In the global picture of an inverse transfer of magnetic helicity, three features can be clearly distinguished through a shell-to-shell transfer analysis:

- a (d)irect (l)ocal (t)ransfer, hereafter "DLT" (figure 5.(b)),
- a (l)ocal (i)nverse (t)ransfer, henceforth "LIT" ($\mathcal{T}_{PPP}^{\mathcal{H}^M}$ curve in figure 5.(a)),
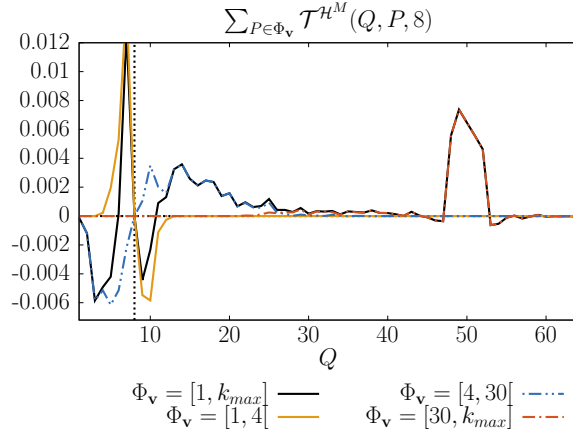
Figure 6. Magnetic helicity transfer rates to shell $K_0 = 8$, mediated by certain velocity shells at the instant when $\mathcal{I}_{\mathcal{H}^M} = \frac{L}{10}$.

- a (n)on-(l)ocal (i)nverse (t)ransfer from the magnetically-forced scales, called "NLIT" in the following (figure 5.(c)).

A helical decomposition allows to determine which helical contributions play the biggest roles. In the case of the M8c run, the PPP and PCP terms, which correspond to $s_K = s_Q = P$ and $s_P \in \{P, C\}$ respectively, are the dominant terms. As shown in figure 5, while the NLIT is carried out by both terms in a comparable manner, the LIT is essentially done by the PPP term and the DLT predominantly by the PCP one.

Furthermore, these three features can also be associated with different mediating velocity shells: the large-scale velocity field ($P \in [1 - 3]$) is responsible for the DLT, the intermediate-scale velocity field ($P \in [4 - 29]$) for the LIT and the small-scale velocity field $P \geq 30$ mediates the NLIT (figure 6).

For the other runs, these three features (DLT, LIT and NLIT) are also present, even though the dominant terms and their relative importance regarding each of these features varies. For the M01s run for example, the PCP term is negligible, and the dominant terms are the PPP and PNP (mediated by the negative helical part of the velocity field) helical contributions. When high compressibility is present however, the DLT is preferentially mediated by the compressive part of the velocity field.

6. Summary and conclusion

The inverse transfer of magnetic helicity has been investigated in the case of highly compressible isothermal MHD turbulence. For all the considered runs, an inverse transfer to large scales occurs. While the magnetic helicity spectral index does not change significantly as compared to the incompressible case when using a purely solenoidal driving up to a RMS Mach number of about 11, significant deviations are visible at relatively low RMS Mach numbers (of the order of 3) for compressively-driven turbulence. When considering the Alfvén velocity helicity spectra however, a spectral index close to the current helicity one in the incompressible case is retrieved. This suggests an extension of the Alfvénic balance found in the incompressible case, which seems well verified for highly compressible flows.

Furthermore, helically-decomposed shell-to-shell transfer analysis reveals three features in the global picture of a magnetic helicity inverse transfer: (*i*) a direct local transfer, preferentially mediated by the compressive part of the velocity field at large scales, (*ii*) an inverse local transfer, preferentially mediated by the positive helical part of the velocity field at intermediate scales and

(*iii*) a non-local inverse transfer from the magnetically-forced scales, mediated by the small-scale velocity field, both positive helical and compressive part of the velocity field playing a significant role.

Acknowledgments

References

[1] A. Alexakis, P. D. Mininni, and A. Pouquet. On the inverse cascade of magnetic helicity. *The Astrophysical Journal 640*, pages 335–343, 2006.

[2] D. Balsara and A. Pouquet. The formation of large-scale structures in supersonic magnetohydrodynamic flows. *Physics of Plasmas Vol. 6 No. 1*, pages 89–99, 1999.

[3] D. S. Balsara. Self-adjusting, positivity preserving high order schemes for hydrodynamics and magnetohydrodynamics. *Journal of Computational Physics 231*, pages 7504–7517, 2012.

[4] M. A. Berger. Introduction to magnetic helicity. *Plasma Physics and Controlled Fusion 41*, pages B167–B175, 1999.

[5] J. W. Bieber, P. A. Evenson, and W. H. Matthaeus. Magnetic helicity of the Parker field. *The Astrophysical Journal, 315*, pages 700–705, 1987.

[6] A. Brandenburg. The inverse cascade and nonlinear alpha-effect in simulations of isotropic helical hydromagnetic turbulence. *The Astrophysical Journal 550*, pages 824–840, 2001.

[7] A. Brandenburg and K. Subramanian. Astrophysical magnetic fields and nonlinear dynamo theory. *Physics Reports 417*, pages 1–209, 2005.

[8] M. Christensson and M. Hindmarsh. Inverse cascade in decaying three-dimensional magnetohydrodynamic turbulence. *Physical Review E 64, 056405*, 2001.

[9] P. Colella and P. R. Woodward. The piecewise parabolic method (PPM) for gas-dynamical simulations. *Journal of Computational Physics 54*, pages 174–201, 1984.

[10] B. G. Elmegreen and J. Scalo. Interstellar turbulence I: Observations. *Annual Review of Astronomy and Astrophysics 42*, pages 211–273, 2004.

[11] W. M. Elsässer. Hydromagnetic dynamo theory. *Reviews of Modern Physics 28, No. 2*, pages 135–163, 1956.

[12] C. R. Evans and J. F. Hawley. Simulation of magnetohydrodynamic flows: a constrained transport method. *The Astrophysical Journal 332*, pages 659–677, 1988.

[13] C. Federrath. On the universality of supersonic turbulence. *Monthly Notices of the Royal Astronomical Society 436*, pages 1245–1257, 2013.

[14] C. Federrath, J. Roman-Duval, R. S. Klessen, W. Schmidt, and M.-M. Mac Low. Comparing the statistics of interstellar turbulence in simulations and observations, solenoidal versus compressive turbulence forcing. *Astronomy and Astrophysics 512, A81*, 2010.

[15] J. Graham, P. D. Mininni, and A. Pouquet. High Reynolds number magnetohydrodynamic turbulence using a Lagrangian model. *Physical Review E 84, 016314*, 2011.

[16] P. Grete, B. W. O'Shea, K. Beckwith, W. Schmidt, and A. Christlieb. Energy transfer in compressible magnetohydrodynamic turbulence. *Physics of Plasmas 24, 092311*, 2017.

[17] A. J. Hundhausen. The solar wind. In M. G. Kivelson and C. T. Russell, editors, *Introduction to Space Physics*, chapter 4. Cambridge University Press, 1995.

[18] M. Linkmann, G. Sahoo, M. McKay, A. Berera, and L. Biferale. Effects of magnetic and kinetic helicities on the growth of magnetic fields in laminar and turbulent flows by helical fourier decomposition. *The Astrophysical Journal 836:26*, 2017.

[19] B. C. Low. Magnetohydrodynamic processes in the solar corona: Flares, coronal mass ejections, and magnetic helicity. *Physics of Plasmas 1*, pages 1684–1690, 1994.

[20] M.-M. Mac Low. The energy dissipation rate of supersonic, MHD turbulence in molecular clouds. *The Astrophysical Journal 524*, pages 169–178, 1999.

[21] S. K. Malapaka. *A Study of Magnetic Helicity in Decaying and Forced 3D-MHD Turbulence*. PhD thesis, Universität Bayreuth, 2009.

[22] P. D. Mininni and A. Pouquet. Finite dissipation and intermittency in magnetohydrodynamics. *Physical Review E 80, 025401*, 2009.

[23] H. K. Moffatt. The degree of knottedness of tangled vortex lines. *Journal of Fluid Mechanics 35*, pages 117–129, 1969.

[24] W.-C. Müller, S. K. Malapaka, and A. Busse. Inverse cascade of magnetic helicity in magnetohydrodynamic turbulence. *Physical Review E 85, 015302*, 2012.

[25] A. Pouquet, U. Frisch, and J. Léorat. Strong MHD helical turbulence and the nonlinear dynamo effect. *Journal of Fluid Mechanics 77, part 2*, pages 321–354, 1976.

[26] P. S. Verma, J.-M. Teissier, O. Henze, and W.-C. Müller. Fourth order accurate finite volume CWENO scheme for astrophysical MHD problems. *Monthly Notices of the Royal Astronomical Society 482*, pages 416–437, 2019.

[27] L. Woltjer. A theorem on force-free magnetic fields. *Proceedings of the National Academy of Sciences 44, No. 6*, pages 489–491, 1958.